Journal of Theoretical Biology 581 (2024) 111756

Contents lists available at ScienceDirect

Journal of Theoretical Biology

journal homepage: www.elsevier.com/locate/yjtbi

A mathematical model of obesity-induced type 2 diabetes and efficacy of anti-diabetic weight reducing drug

Nourridine Siewe [a,*], Avner Friedman [b]

[a] School of Mathematics and Statistics, College of Science, Rochester Institute of Technology, Rochester, NY, USA
[b] Department of Mathematics, The Ohio State University, Columbus, OH, USA

ARTICLE INFO

Keywords:
Type 2 diabetes
GPL-1
GLUT-2/GLUT-4
Glucose
Insulin
Mounjaro
A1C

ABSTRACT

The dominant paradigm for modeling the obesity-induced T2DM (type 2 diabetes mellitus) today focuses on glucose and insulin regulatory systems, diabetes pathways, and diagnostic test evaluations. The problem with this approach is that it is not possible to explicitly account for the glucose transport mechanism from the blood to the liver, where the glucose is stored, and from the liver to the blood. This makes it inaccurate, if not incorrect, to properly model the concentration of glucose in the blood in comparison to actual glycated hemoglobin (A1C) test results. In this paper, we develop a mathematical model of glucose dynamics by a system of ODEs. The model includes the mechanism of glucose transport from the blood to the liver, and from the liver to the blood, and explains how obesity is likely to lead to T2DM. We use the model to evaluate the efficacy of an anti-T2DM drug that also reduces weight.

1. Introduction

Obesity is a major driver of type 2 diabetes mellitus (T2DM): Approximately 85% of adults in the United States diagnosed with type 2 diabetes are either overweight or obese, and about 30% of obese individuals are affected by this condition. Studies (Zaki et al., 2020) have identified causes and mechanisms which make obesity a high risk for T2DM. Based on these studies, we develop in this paper a mathematical model that explains how obesity is likely to lead to T2DM. The model is also used to evaluate the efficacy of an anti-T2DM drug, which is also weight reducing.

The model variables include glucose, insulin and hormone GLP-1 that is produced after a meal, protein transporters GLUT-2 and GLUT-4, fatty acids NEFA, glycogen ('stored' glucose in the liver) and glucagon (which converts glycogen to glucose) and pancreatic β-cells and α-cells.

In obese patients, adipose tissue releases a high amount of NEFA (non-esterified ('free') fatty acids), and it was suggested that NEFA is responsible for insulin resistance (Karpe et al., 2011; Zhou et al., 2020; Lu et al., 2016) and inflammation (Zhou et al., 2020). The inflammatory acids in NEFA are mainly palmitic and stearic acids (Zhou et al., 2020; Lu et al., 2016; Fraser et al., 1999), while the inflammation reducing acids are primarily oleic and linoleic acids (Fraser et al., 1999; Heskey et al., 2016; Salvadó et al., 2013). The inflammatory acids promote β-cells dysfunction and T2DM, while oleic and linoleic acids reduce the inflammation (Heskey et al., 2016). In the sequel we represent the inflammatory acids by palmitic acid, and the inflammation reducing acids by oleic acid.

Hormone GLP-1 (glucagon-like peptide 1) is released from the gut enteroendocrine cells within minutes of the nutrient ingestion. GLP-1 stimulates pancreatic β-cells to secrete insulin. As insulin enters the liver and muscle cells, it activates GLUT-4 (membrane-protein glucose transporter type 4) through IRS-1-PI3K-Akt signaling. GLUT-4 then transports glucose from the outside to inside cells, thus clearing glucose from the blood into liver and muscle cells, under inducement by insulin Cohen et al. (1978), where it is stored primarily by liver cells, as glycogen (Villanueva-Peñacarrillo et al., 2001; Green et al., 2012; Drucker, 2018; Mukherjee et al., 2013). Metabolic activities over an extended time (e.g., 6–7 h after a meal) result in hypoglycemia Rehni and Dave (2018). Hypoglycemia, or low blood sugar, can be a dangerous and potentially life-threatening condition, especially for individuals with diabetes (Agrawal et al., 2022). Hypoglycemic conditions stimulate pancreatic α-cells to secrete glucagon (Kawamori, 2017; Jacobson et al., 2009). Glucagon enters the liver, where it induces glycogen to become glucose (Ogilvy-Stuart and Beardsall, 2020), which is then transported, by GLUT-2, from the liver to the blood (Gupta, 2022; Hosokawa and Thorens, 2002). The hormone GLP-1 suppresses glucagon secretion by α-cells when glucose level is high, but increases it when glucose level is low (Zhang et al., 2019). T2DM is a disease characterized by β-cells dysfunction in production of insulin, or in failure to use it effectively (insulin resistance).

* Corresponding author.
E-mail address: nourridine@aims.ac.za (N. Siewe).

https://doi.org/10.1016/j.jtbi.2024.111756
Received 17 August 2023; Received in revised form 4 November 2023; Accepted 26 January 2024
0022-5193/© 2024 Published by Elsevier Ltd.

NEFA is stored in adipose tissue, but during a meal it is released from its suppressed form (Frayn, 1998), by a process that involves insulin Jelic et al. (2009), Virtamen (2019). The released NEFA is inflammatory, and since palmitic acid is the most common acid in the human body (Carta et al., 2017), we shall represent the released NEFA by increased release of palmitic acid from adipose tissue.

Elevated NEFA contributes to impaired response to GLP-1 (Drucker, 2018) and prolonged exposure to palmitic acid increases β-cells apoptosis (Oh et al., 2018). Palmitic acid was also shown to induce insulin resistance in obese individuals (Chandra et al., 2021) through AMPK-dependent mechanism, and to promote inflammatory cytokines, such as tumor necrotic factor α (TNF-α) (Carta et al., 2017; Qiu et al., 2022). TNF-α induces insulin resistance by triggering a cascade of events. It starts with PTEN (phosphatase and tensin homolog deleted on chromosome ten) modulation, which reduces Akt (also known as protein kinase B) activity (da Costa et al., 2016). Reduced Akt activity then impairs the translocation of GLUT-4 to the cell membrane, resulting in decreased glucose uptake. Additionally, TNF-α leads to the conversion of IRS-1 (insulin receptor substrate 1) into an inhibitor of insulin receptor kinase activity, disrupting the normal insulin signaling cascade (Plomgaard et al., 2005).

Modest reduction of NEFA, in T2DM, can be achieved by appropriate diets (Samkani et al., 2018). There are several drugs that decrease postprandial NEFA, such as rosiglitazone liraglutide (Chen et al., 2018). There are also drugs that mimic the hormone activity of GLP-1 (GLP-1 receptor agonists), and stimulate β-cells to produce more insulin Castro (2022), e.g., liraglutide and semaglutide (Knudsen and Lau, 2019). A review of pharmacological and clinical factors that may influence GLP-1 receptor agonists in management of T2DM and obesity is given in Klein and Dolzan (2022). Mounjaro and Ozempic are two drugs that stimulate insulin secretion by activating GLP-1 receptor to target GLP-1, and reduce glucagon level (Puddick et al., 2023). They also delay gastric emptying (Lynch and Llano, 2023), that is, slow down fast food travel through the digestive system, which can lead to a reduction in adipose tissue and NEFA in some individuals, and in turn help to lose weight (Puddick et al., 2023).

The majority of glycogen is stored in skeleton muscles (~500 g) and the liver (~100 g) (Jensen et al., 2011). The delivery of glucose from the blood to muscle cells consists of different regulatory steps than in the delivery of glucose from the blood to the liver; it is mostly independent of GLUT-4 transporter (Richter, 2021). Glycogenolysis in muscle cells provide glucose to the cells (BD Editors, 2017), which they use for ATP synthesis (El Bacha et al., 2010). In this paper we focus on glucose transport to the liver. We develop a mathematical model to study glucose clearance in obese adults by combination of NEFA reduction and GLP-1 receptor agonist, as in the experimental paper (Kang et al., 2013). Adipose tissue directs macrophages towards the pro-inflammatory phenotype that secrete inflammatory cytokines, including TNF-α, IL-6, IL-1β, IL-12 and IL-23 (Lauterbach and Wunderlich, 2017; Castoldi et al., 2016). To simplify the model we take TNF-α to represent all these cytokines, and do not include macrophages explicitly in the model.

There are many ODE models of glucose dynamics. A comprehensive review of glucose-insulin systems, up to 2013, is given in Palumbo et al. (2013). Article (Ortuno and Rojas, 2015) introduces a system of glucose, insulin, β-cells and insulin receptor, and studies the stability of an equilibrium state. In Nani and Jin (2015), T2DM simulations are given for a system consisting of glucose, glycogen, glucagon, and insulin. A more complex system consisting of 28 equations is introduced in López-Palau and Olais-Govea (2020). An extensive 2020 review of physiological and clinical investigations of glucose dynamics in homeostasis and diabetes is given in Mari et al. (2020). A more recent paper deals with the dynamics of glucose and glycerol (produced by adipose tissue Hampton et al., 2022). A model in Boutayeb et al. (2015) includes Free Fatty Acid (FFA) in the glucose-insulin system: two stable equilibrium points represent normal and diabetic states, and a third unstable equilibrium point suggests transition from normal state to diabetes when FFA is increased. But all the above papers do not explicitly account for the glucose transport mechanism from the blood to the liver, where glucose is stored, and from the liver to blood. This makes it inaccurate, or incorrect, to properly model glucose dynamics in the blood.

In Section 2, we develop a model of glucose dynamics. In Section 3 we simulate the model, first in health, and then in people who are becoming obese, which increases their risk of becoming diabetic. In Section 4 we use the model to simulate treatment of T2DM with a drug that also reduces weight. The conclusion of the paper is in Section 5, sensitivity analysis in Section 6, and parameter estimations in Section 7.

Table 1
Variables of the model. Densities and concentrations in units of g/cm^3.

Variables	Descriptions	Variables	Descriptions
A	Density of α-cells	B	Density of β-cells
G	Glucose	G^*	Liver glucose
C	Glucagon	G^{**}	Liver glycogen
I	Insulin	L	GLP-1
U_2	GLUT-2	U_4	GLUT-4
P	Palmitic acid	O	Oleic acid
T_α	TNF-α	D	Mounjaro

2. Mathematical model

The mathematical model in health and obesity is based on the networks shown in Fig. 1, which depict the effect of NEFA on insulin. In health, the food intake is moderate and the effect of NEFA on palmitic acid is at normal healthy level. But, if food intake is abnormally high for a long time (e.g., several years), a person is becoming obese, and obesity significantly increases the effect of NEFA on palmitic acid. Table 1 lists the variables of the model in units of g/cm^3, and Table 2 lists the model parameters with their respective units and sources. All equations are in the blood, except the equation of "stored glucose" in the liver.

The function

$$F(t;t_0,t_1)=\begin{cases}1, & \text{if } t_0\le t\le t_1 \ (t_0,\ t_1 \text{ in hours})\\ 0, & \text{otherwise.}\end{cases} \tag{2.1}$$

will be used to describe the direct effect of food-intake at time $t=0$ on L, G, G^*, O and P.

When a species Z is enhanced by a species X or inhibited by another species Y, we will express the rates of these effects by the Michaelis–Menten law, $Z\dfrac{X}{K_X+X}$ and $Z\dfrac{1}{1+Y/\hat{K}_Y}$, respectively.

Equation for GLP-1 (L)

GLP-1 satisfies the following equation:

$$\frac{dL}{dt}=\lambda_L(t)-\mu_{LB}BL-\mu_{LA}AL, \tag{2.2}$$

where $\lambda_L(t)=\gamma_L F(t;0,1)$ is a source of GLP-1 produced by food intake, and μ_{LB}, μ_{LA} are reduced rates of GLP-1 through interacting with receptors on β-cells and α-cells, respectively.

Equations for α-cells (A) and β-cells (B)

GLP-1 activates β-cells. Chronic exposure to elevated level of glucose and NEFA (in particular, palmitic acid Oh et al., 2018) causes β-cell dysfunction and increased apoptosis (Cnop et al., 2005). We write the equation for β-cells in the following form:

$$\frac{dB}{dt}=\tilde{\lambda}_B\frac{(L-L_0)^+}{K_L+(L-L_0)^+}-\tilde{\mu}_B B(1+\xi_1 G+\xi_2 P), \tag{2.3}$$

where $\tilde{\lambda}_B$ is an activation rate, $\tilde{\mu}_B$ is a deactivation rate, and ξ_1, ξ_2 are rates of β-cells impairments by glucose and palmitic acid. L_0 is the threshold of L below which it fails to activate β-cells.

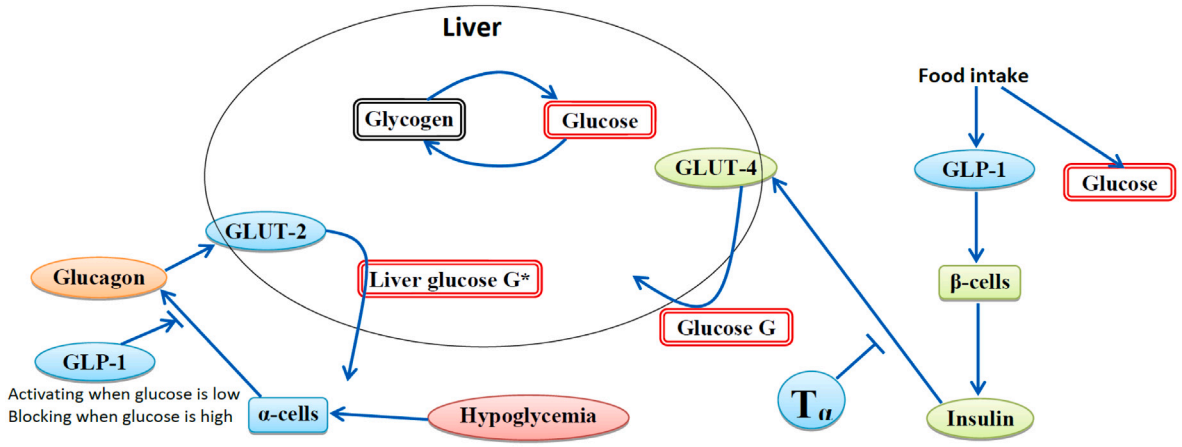

(a) Network of cells and cytokines, that are involved in glucose dynamics.

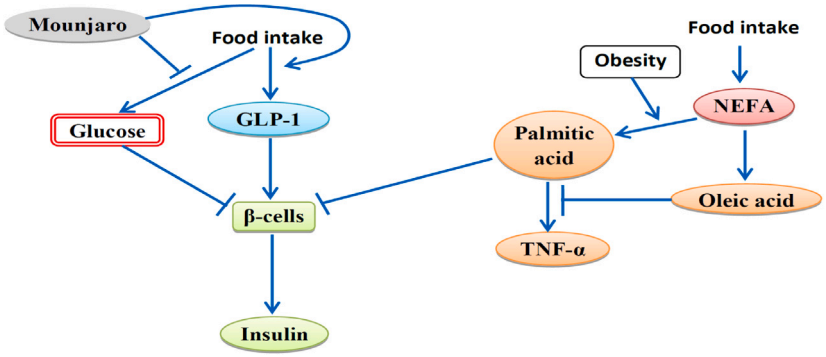

(b) Effects of NEFA and obesity on the network in Figure 1a. Palmitic acid and oleic acid have been added, with their suppressive effect on β-cells and GLUT-4 by TNF-α. Obesity increases production of palmitic acid.

Fig. 1. Networks of the model without NEFA effect (Fig. 1(a)) **and with NEFA effect** (Fig. 1(b)). The cells are represented by fully colored square nodes, hormones and cytokines/chemokines by circular nodes, and glucose by square nodes with double borders. Glucose in the blood is represented by red color and glucose in the liver (glycogen) by black color. The greenish nodes indicate the variables that derive from or interact directly with the β-cells. The nodes with blueish colors indicate the variables that derive from or interact directly with the α-cells. The orange nodes represent variables that are led by the NEFA pathway.

α-cells are activated in hypoglycemia, but GPL-1 blocks their activation, so that

$$\frac{dA}{dt} = \tilde{\lambda}_A \frac{(I_{\text{hypo}} - I)^+}{K_I + (I_{\text{hypo}} - I)^+} \frac{1}{1 + L/\hat{K}_L} - \tilde{\mu}_A A, \tag{2.4}$$

where $\tilde{\lambda}_A$ and $\tilde{\mu}_A$ are activation and deactivation rates, and I_{hypo} is a critical level of insulin, below which α-cells are activated.

Equation for insulin (I)

Insulin is secreted by β-cells and is degraded, at rate μ_I, through interaction with receptors in the liver. Insulin is also lost when it connects with insulin receptors in the liver, to start a signaling cascade that results in activating GLUT-4 (Huang et al., 2001). We write the equation of I as follows:

$$\frac{dI}{dt} = \lambda_{IB} B - \mu_I I - \mu_{IG} G I, \tag{2.5}$$

where μ_{IG} is constant.

Equation for GLUT-2 (U_2) and GLUT-4 (U_4)

GLUT-2 is activated by glucagon, and GLUT-4 is activated by insulin. TNF-α induces insulin resistance, resulting in GLUT-4 deactivation (Plomgaard et al., 2005). Hence,

$$\frac{dU_2}{dt} = \lambda_{U_2 C} C - \mu_{U_2} U_2, \tag{2.6}$$

$$\frac{dU_4}{dt} = \lambda_{U_4 I} I \frac{1}{1 + \eta_{T_\alpha} T_\alpha} - \mu_{U_4} U_4, \tag{2.7}$$

where μ_{U_2} and μ_{U_4} are degradation rates of U_2 and U_4, respectively. The parameter η_{T_α} represents an inhibiting-effect of TNF-α on GLUT-4.

Equations for glucagon (C), blood glucose (G) and 'stored' glucose (G^*)

Glucagon is secreted by α-cells (Kawamori, 2017); GLP-1 suppresses its production if glucose level is high, and in turn increases its production if glucose level is low (Zhang et al., 2019). We accordingly have:

$$\frac{dC}{dt} = \frac{\lambda_{CA} A}{1 + \gamma_1 H(G - \xi_4) L} (1 + \gamma_2 H(\xi_3 - G) L) - \mu_C C, \tag{2.8}$$

for some parameters γ_1, γ_2, ξ_3 and ξ_4, where $H(x) = 1$ if $x > 0$ and $= 0$ otherwise, and μ_C is the rate of loss of C through binding with receptors in the liver.

We denote the rates of glucose production during food intake by $\lambda_G(t)$, and the rate of glucose elimination in the first 2 h by $\lambda_{G^*}(t)$. Glucose is transported by U_4 from the blood into the liver and by U_2 from the liver to the blood at rates λ_{GU_4} and $\lambda_{G^*U_2}$, respectively. We accordingly have,

$$\frac{dG}{dt} = \lambda_G(t) - \lambda_{G^*}(t) G + \lambda_{G^*U_2} G^* \frac{U_2}{K_{U_2} + U_2} - \lambda_{GU_4} G \frac{U_4}{K_{U_4} + U_4}. \tag{2.9}$$

We take $\lambda_G(t) = \gamma_G F(t; 0, 1)$, and $\lambda_{G^*}(t) = \gamma_{G^*} F(t; 1, 3)$, where γ_G and γ_{G^*} are constants.

Glycogenesis is the process of synthesizing glycogen in liver (Patino and Orrick, 2023). It is the primary way in which the body stores

Table 2
Parameters for the model.

Parameters	Descriptions	Values	References
K_L	Half-saturation of GLP-1	1.7×10^{-14} g/cm^3	est.
$\hat{K}_L$	Inhibitory-saturation by GLP-1	1.7×10^{-14} g/cm^3	est.
K_{U_2}	Half-saturation of GLUT-2	9.45×10^{-6} g/cm^3	Wolfsdorf and Weinstein (2012)est.
K_{U_4}	Half-saturation of GLUT-4	2.78×10^{-6} g/cm^3	Gorovits and Charron (2003)est.
K_I	Half-saturation of insulin	2×10^{-13} g/cm^3	est.
$\hat{K}_O$	Inhibitory-saturation of P by O	1.36×10^{-6} g/cm^3	est.
$\tilde{\lambda}_A$	Activation rate of A	0.35 d^{-1}	est.
$\tilde{\lambda}_B$	Activation rate of B	1.745×10^{9} d^{-1}	est.
γ_L	Baseline secretion rate of GLP-1	1.98×10^{-13} g/cm^3 d^{-1}	est.
λ_{IB}	Secretion rate of insulin by B	1.26×10^{-8} d^{-1}	est.
λ_{U_4I}	Secretion rate of GLUT-4 by I	4.17×10^{7} d^{-1}	est.
λ_{U_2C}	Secretion rate of GLUT-2 by C	6.6×10^{10} d^{-1}	est.
λ_{CA}	Secretion rate of glucagon by A	1.65×10^{-11} d^{-1}	est.
γ_G	Baseline secretion rate of glucose	0.017 g/cm^3 d^{-1}	est.
γ_{G^*}	Baseline rate of early glucose elimination	11.1 d^{-1}	est.
γ_O	Baseline secretion rate of oleic acid	1.46×10^{-4} g/cm^3 d^{-1}	est.
γ_P	Baseline secretion rate of palmitic acid	1.83×10^{-6} g/cm^3 d^{-1}	est.
$\hat{\gamma}_P$	Baseline obesity-prone secretion rate of palmitic acid	5.72×10^{-5} g/cm^3 d^{-1}	est.
λ_{GU_4}	Transportation rate of glucose by U_4	1.548 d^{-1}	Assumed
$\lambda_{G^*U_2}$	Importation rate of liver-glucose by U_2	4.644 d^{-1}	Assumed
λ_{T_α}	Normal secretion rate of TNF-α	1.19×10^{-9} g/cm^3 d^{-1}	est.
$\lambda_{T_\alpha P}$	Secretion rate of TNF-α by palmitic acid	3.26×10^{-4} d^{-1}	est.
μ_A	Deactivation rate of A	8.32 d^{-1}	Finegood et al. (1995), Butler et al. (2007)est.
μ_B	Deactivation rate of B	8.32 d^{-1}	Cerf (2013), Jones et al. (2015), Finegood et al. (1995)est.
μ_{LB}	Absorption rate of GLP-1 by B	251 cm^3/g d^{-1}	Sharma et al. (2018)est.
μ_{LA}	Absorption rate of GLP-1 by A	251 cm^3/g d^{-1}	Sharma et al. (2018)est.
μ_I	Decay rate of insulin	198.04 d^{-1}	Morishima et al. (1992), Duckworth (1988)est.
μ_{U_4}	Decay rate of GLUT-4	1.85 d^{-1}	Host et al. (1998), Schnurr et al. (2015)est.
μ_{U_2}	Decay rate of GLUT-2	4.62 d^{-1}	Hou et al. (2009)est.
μ_C	Decay rate of glucagon	166.22 d^{-1}	Norman and Litwack (1997)est.
μ_{T_α}	Decay rate of TNF-α	199 d^{-1}	Simo et al. (2012), Siewe and Friedman (2020)est.
μ_O	Degradation rate of oleic acid	13.68 d^{-1}	Li et al. (2023), Nabors et al. (1984)est.
μ_P	Degradation rate of palmitic acid	12 d^{-1}	Li et al. (2023), Nabors et al. (1984)est.
μ_D	Degradation rate of mounjaro	0.139 d^{-1}	Lilly (2022)
μ_{IG}	Baseline decay rate of I by G	6×10^{5} d^{-1}	est.
γ_1	Blocking rate of glucagon	10^{-14}	est.
γ_2	Inducing rate of glucagon	1.2×10^{-14}	est.
ξ_1	Deactivation rate of B by G	1×10^{12} cm^3/g	est.
ξ_2	Deactivation rate of B by P	1×10^{12} cm^3/g	est.
ξ_3	Switch level of G for inhibition of C-secretion	10^{-2} g/cm^3	est.
ξ_4	Switch level of G for activation of C-secretion	10^{-4} g/cm^3	est.
η_{T_α}	Rate of inhibiting-effect of TNF-α on GLUT-4	10^{10} cm^3/g	est.
K_D	Half-saturation of G by D	10^{-7} cm^3/g	est.
$\hat{K}_D$	Inhibitory-saturation of G by D	10^{-7} cm^3/g	est.
I_{hypo}	Level of I in hypoglycemia	8×10^{-14} g/cm^3	Buppajarntham et al. (2021), Melmed et al. (2016)est.

est.= this parameter was estimated in Section 7.

glucose for short-term energy needs. Glycolysis is the breakdown of glucose into two molecules of pyruvate (three-carbon acid), a simpler compound (Patino and Orrick, 2023). It is the first stage of glucose metabolism and occurs in the cytoplasm of cells. The process of glycogenesis ($G^* \to G^{**}$) and the process of glycolysis ($G^{**} \to G^*$) are enzymatic processes, and, for simplicity, we take $G^{**} = G^*$ and view G^* as "stored glucose". We assume that the blood glucose loss at rate $\frac{dG}{dt} = -\lambda_{G^*}(t)G$ entered the liver; hence,

$$\frac{dG^*}{dt} = \lambda_{G^*}(t)G + \lambda_{GU_4}G\frac{U_4}{K_{U_4}+U_4} - \lambda_{G^*U_2}G^*\frac{U_2}{K_{U_2}+U_2}, \tag{2.10}$$

Equation for oleic acid (O) and palmitic acid (P)

Oleic and palmitic acids are coming from the food source. We take

$$\frac{dO}{dt} = \lambda_O(t) - \mu_O O \qquad \text{and} \qquad \frac{dP}{dt} = \lambda_P(t) - \mu_P P, \tag{2.11}$$

where $\lambda_O(t) = \gamma_O F(t;0,1)$ and $\lambda_P(t) = (\gamma_P + \hat{\gamma}_P)F(t;0,1)$; μ_O and μ_P are the rates by which O and P are, respectively, removed from the blood. The parameters γ_O and γ_P, in health, are increased by the same factor in obesity, while $\hat{\gamma}_P = 0$ in health and $\hat{\gamma}_P > 0$ in obesity (as indicated in Fig. 1(b)).

Equation for TNF-α (T_α)

Palmitic acid promotes TNF-α (Zhou et al., 2020; Lu et al., 2016; Fraser et al., 1999; Carta et al., 2017; Qiu et al., 2022), but oleic acid blocks it (Fraser et al., 1999; Heskey et al., 2016; Salvadó et al., 2013). Hence,

$$\frac{dT_\alpha}{dt} = \lambda_{T_\alpha} + \lambda_{T_\alpha P}P\frac{1}{1+O/\hat{K}_O} - \mu_{T_\alpha}T_\alpha, \tag{2.12}$$

where μ_{T_α} is the degradation rate of T_α.

Type 2 diabetes is usually diagnosed by the glycated hemoglobin (A1C) test. When sugar enters the blood system, it attaches to hemoglobin. In the A1C test, the percentage of red blood cells that are sugar-coated is measured, and the results are interpreted as follows CDC (2022):

Normal:	below 5.7%,
Prediabetes:	5.7 to 6.4%,
Diabetes:	above 6.4%.

The test indicates the average glucose level in blood over 3 months.

The relation between the A1C percentage and the concentration of glucose in blood (eAG) is given by the formula $28.7 \times \text{A1C} - 46.7 =$

Table 3
Glucose level during the first 2–3 h post-meal.
Source: From Vieira (2022) (Fig. 4).

Normal	Fasting	Less than 100 mg/dL= 10^{-3} g/cm^3
	1–2 h after meal	Less than 140 mg/dL= 1.4×10^{-3} g/cm^3
	2–3 h after eating	Less than 100 mg/dL
Prediabetes	Fasting	100 to 125 mg/dL= 1.25×10^{-3} g/cm^3
	2 h after meal	140–199 mg/dL= 1.99×10^{-3} g/cm^3
Type 1 or 2 diabetes	Fasting	126 gm/dL= 1.26×10^{-3} g/cm^3 or higher
	2 h after meal	200 mg/dL= 2×10^{-3} g/cm^3 or higher

Table 4
The level of natural insulin in humans, after glucose administration.
Source: From Buppajarntham et al. (2021) and Melmed et al. (2016).

	Insulin level (pmol/L)	Insulin level (g/cm^3)
Fasting	< 174	$< 0.97\times10^{-13}$
30 min after glucose administration	208–1597	$1.16–8.88\times10^{-13}$
1 h after glucose administration	125–1917	$0.7–10.66\times10^{-13}$
2 h after glucose administration	111–1153	$0.62–6.41\times10^{-13}$
≥ 3 hours after glucose administration	< 174	$< 0.97\times10^{-13}$

Where 1 mol/L= 5.56×10^{-4} g/cm^3.

eAG (American Diabetes Association, 2022). Accordingly, the A1C results can be interpreted as follows:

$$\begin{aligned} &\text{Normal:} && \text{below } 117 \text{ mg/dL} = 1.17\times10^{-3} \text{ g/cm}^3,\\ &\text{Prediabetes:} && 117 \text{ to } 137 \text{ mg/dL} = 1.37\times10^{-3} \text{ g/cm}^3, \qquad (2.13)\\ &\text{Diabetes:} && \text{above } 137 \text{ mg/dL}. \end{aligned}$$

When A1C test is not available, another common test is the fasting blood sugar test (FBST). The blood test is taken after overnight fast, and the results are given in term of the concentration of glucose in blood Riley (2022):

$$\begin{aligned} &\text{Normal:} && \text{below } 100 \text{ mg/dL} = 10^{-3} \text{ g/cm}^3,\\ &\text{Prediabetes:} && 100 \text{ to } 125 \text{ mg/dL} = 1.25\times10^{-3} \text{ g/cm}^3, \qquad (2.14)\\ &\text{Diabetes:} && \text{above } 125 \text{ mg/dL}. \end{aligned}$$

Note that these numbers which represent average glucose concentration in blood over the past 3 months are larger than the corresponding numbers in (2.14), which are obtained after overnight fasting.

In numerical simulations of the model, we shall compare our results with data given below, in Tables 3 and 4. We shall also use simulations to diagnose patients for diabetes, using the standard A1C test.

3. Numerical results

Healthy (non-obese) case

In Fig. 2 we simulated the profile of the model variables for 12 h in a case of an individual without diabetes or obesity. After a normal fasting period, the person takes a meal at time $t = 0$, but no additional meal for the following 12-h period. We see that the glucose level (G) at $t = 0$ is less than 10^{-3} g/cm^3 = 100 mg/dL; it increases to nearly 1.3×10^{-3} g/cm^3 (less than 140 mg/dL) after 2 h, and drops to 100 mg/dL after 3 h. This is in agreement with Table 3, and with FBST test for a healthy person. The range of glucagon (C) is in agreement with the bounds derived in Section 7 (Parameter Estimations).

The profile of glycogen (G^*, "stored glucose") follows the profile of glucose with some delay: it continues to increase until the 4 h mark, and then gradually decreases. The total sugar energy, $E = G + G^*$, increases immediately after a meal, and then gradually decreases due to the metabolic activity of the person.

The level of insulin (I) in Fig. 2 increases for the first 2–3 h, reaching a maximum of 12×10^{-13} g/cm^3, and then it starts decreasing, to less than 0.1×10^{-13} g/cm^3 after 6 h. In Table 4, insulin level reaches maximum 10^{-3} g/cm^3, 1 h after glucose administration, and decreases below 0.1×10^{-13} g/cm^3 after 3 h. The reason the insulin profile in our case is slower to increase to its maximum and to decrease below 0.1×10^{-13} g/cm^3 can be explained by the fact that the production of insulin, in our case, depends on the activation of β-cells (B), which take some time to increase (after meal) and to decrease, as seen in Fig. 2. The relatively small difference in the maximum levels of I in our simulations vs. data in Table 4 is just a consequence of the amount of food taken at $t = 0$.

In Fig. 2, GPL-1 (L) increases for 2 h after meal, then decreases to its initial level $t = 6$ h (near a time when a person typically would take another meal); without another meal, L continues to drop for the remaining 6 h. The profile of β-cells follows that of L, as it should be. The initial concentration of α-cell profile (A) is high at $t = 0$, since a person, 12 h post-meal, is in a state of hypoglycemia. After a meal at $t = 0$ h, A begins to decrease as the state of hypoglycemia is improved, but at $t = 7$ h, a time when a person typically takes a second meal, A starts increasing continuously, since there is no second meal in the test simulated in Fig. 2.

We finally note that the profile of U_4, which is activated by insulin, and of U_2, which is activated by glucagon, have the same qualitative features as the profiles of I and C, respectively.

A1C test

We can implement the A1C test with our model by simulating the glucose dynamics for 3 months and taking the average of glucose over that period.

We consider a healthy individual who takes three meals per day, 6 h between meals, as shown in Fig. 3.

Taking a meal means an intake of glucose (new λ_G), oleic acid (new λ_O), palmitic acid (new λ_P) and GLP-1 (new λ_L) at the time the meal is taken. The first meal is taken at $t = 0$ The second meal is taken at $t = 6$ h with initial conditions of all variables taken from the profiles of the first meal at $t = 6$ h. We follow the same procedure with the third meal, which is taken at $t = 12$ h.

Fig. 4 simulates the case where the amount of food intake at breakfast and lunch is as in Fig. 2, while the amount of food intake at dinner is twice the amount taken at breakfast or at lunch. We see that the density of β-cells and glucose level increase after each meal. A state of hypoglycemia exists before the first meal and six hours after the last meal; this explains the profile of α-cells, which decreases for the first few hours, and remains low until about $t = 18$ h, and then begins to increase. We note that the profile of the stored glucose (G^*) and the total energy (E) are oscillating, but on the rise, in the first 14 h, and then glucose (G) and total energy are steadily decreasing. According to

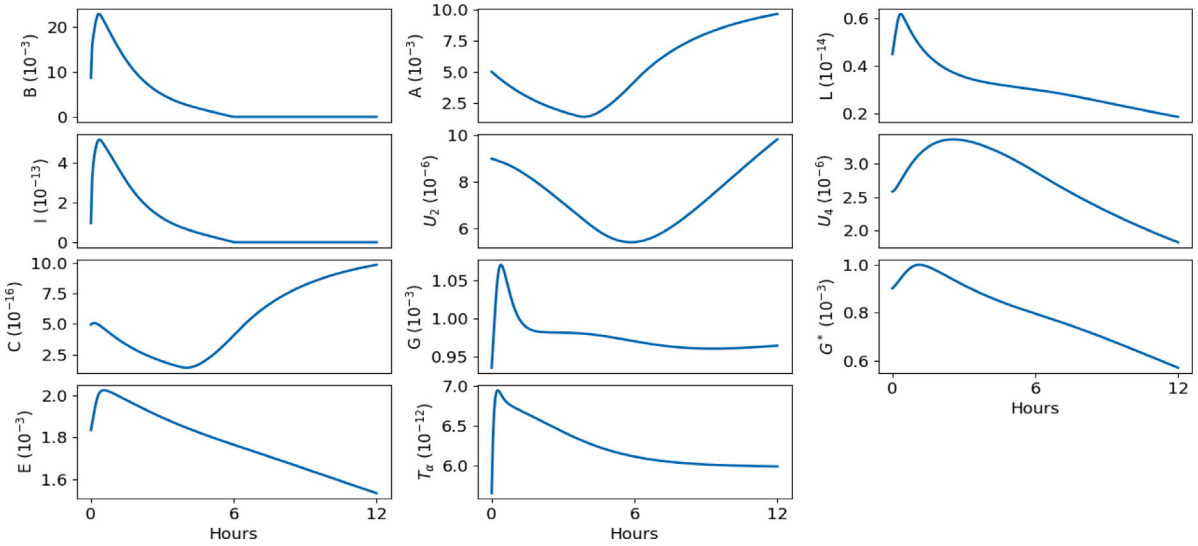

Fig. 2. All variables in health (no diabetes and no obesity), with parameters $\gamma_G = 0.017$ g/cm^3 d^{-1}, $\gamma_L = 1.98 \times 10^{-13}$ g/cm^3 d^{-1}, $\gamma_O = 1.46 \times 10^{-4}$ g/cm^3 d^{-1}, $\gamma_P = 1.83 \times 10^{-6}$ g/cm^3 d^{-1} and $\hat{\gamma}_P = 0$, as in Table 2. $E = G + G^*$ is the total energy from a meal intake; units are in g/cm^3.

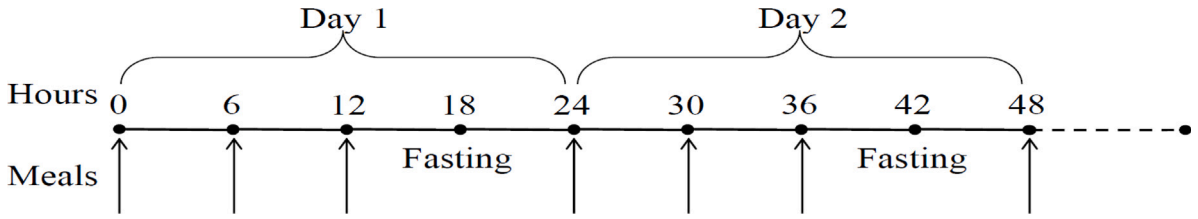

Fig. 3. Schedules for food intake. There are three meals per day: at $t = 0,\ 6,\ 12$ h. The first two meals (breakfast and lunch) are 2 times lighter than the third (dinner).

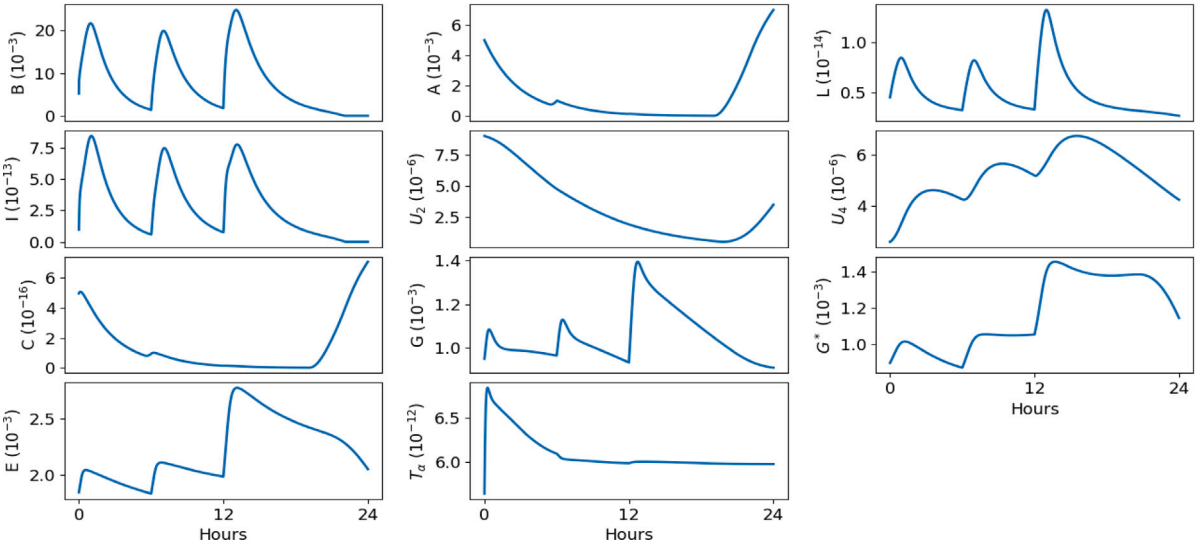

Fig. 4. One day, 3 meals per day with normal health: Profiles of all variables with meal intake as in Fig. 3. $E = G + G^*$ is the total energy from the meals intake. We take $\gamma_G = 0.017$ g/cm^3 d^{-1}, $\gamma_L = 1.98 \times 10^{-13}$ g/cm^3 d^{-1}, $\gamma_O = 1.46 \times 10^{-4}$ g/cm^3 d^{-1}, $\gamma_P = 1.83 \times 10^{-6}$ g/cm^3 d^{-1} and $\hat{\gamma}_P = 0$ for breakfast ($t = 0$ h) and lunch ($t = 6$ h), and $\gamma_G = 2 \times 0.017$ g/cm^3 d^{-1}, $\gamma_L = 2 \times 1.98 \times 10^{-13}$ g/cm^3 d^{-1}, $\gamma_O = 2 \times 1.46 \times 10^{-4}$ g/cm^3 d^{-1}, $\gamma_P = 2 \times 1.83 \times 10^{-6}$ g/cm^3 d^{-1} and $\hat{\gamma}_P = 0$ for dinner ($t = 12$ h); units are in g/cm^3.

Table 3, the profile of glucose, which is more clearly shown in Fig. 5, is that of a non diabetic/non obese individual.

Fig. 6 is an extension of the one-day profile of G to 30 days, where we used the same parameters and initial data as in Fig. 4. Fig. 6 shows that the glucose continuous profile is nearly periodic from one day to another, while the 24-h profile undergoes tiny variations in the first 10 days, before it stabilizes. These variations are the result of the choice of initial conditions, which may vary from one individual to another.

Glucose dynamics during days 30–60 remain the same as in days 20–30 (not shown here), so the average of glucose over 3 months is appropriately 0.86 g/cm^3, or 86 mg/dL. By the A1C test (see Eq. (2.13)), this is a healthy normal case.

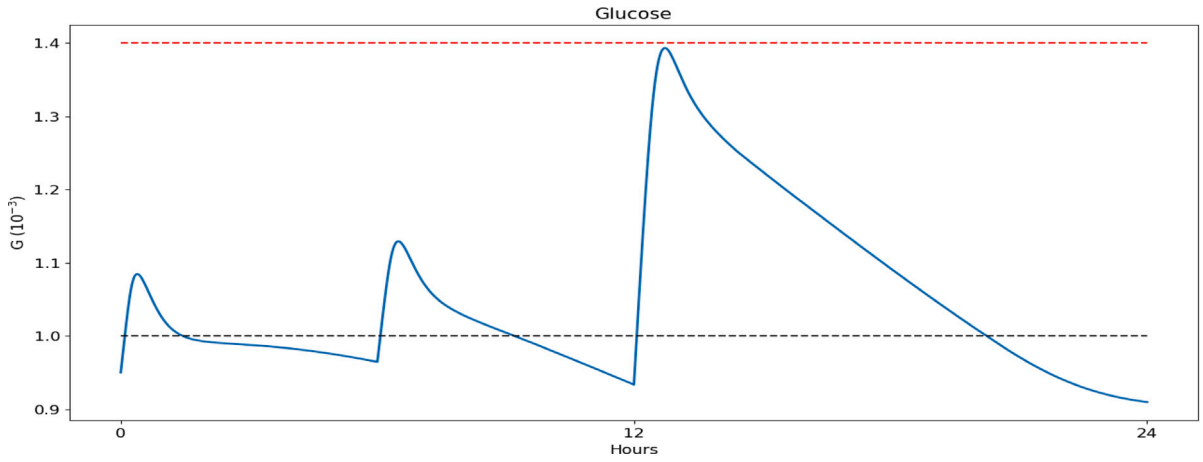

Fig. 5. One day, 3 meals per day: Profiles of glucose from Fig. 4 with $\gamma_G = 0.017$ g/cm^3 d^{-1}, $\gamma_L = 1.98\times10^{-13}$ g/cm^3 d^{-1}, $\gamma_O = 1.46\times10^{-4}$ g/cm^3 d^{-1}, $\gamma_P = 1.83\times10^{-6}$ g/cm^3 d^{-1} and $\hat{\gamma}_P = 0$ for breakfast and lunch, and $\gamma_G = 2\times0.017$ g/cm^3 d^{-1}, $\gamma_L = 2\times1.98\times10^{-13}$ g/cm^3 d^{-1}, $\gamma_O = 2\times1.46\times10^{-4}$ g/cm^3 d^{-1}, $\gamma_P = 2\times1.83\times10^{-6}$ g/cm^3 d^{-1} and $\hat{\gamma}_P = 0$ for dinner. G in units of g/cm^3.

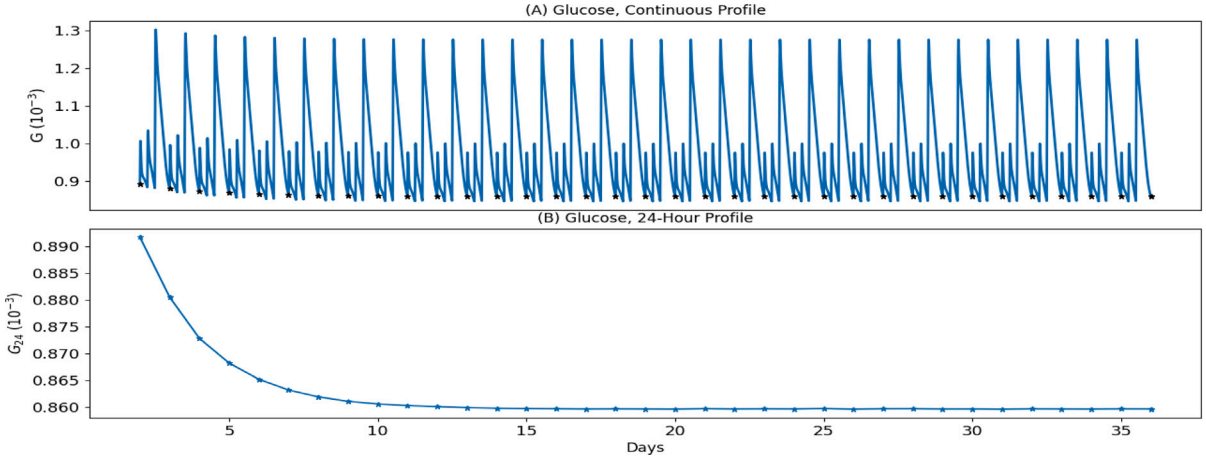

Fig. 6. Thirty days, 3 meals per day: Glucose level in the blood in (A) continuous profile (G), and (B) 24-h profile (G_{24}). The dots represent the daily average of glucose in the blood. Meal intake is as in Fig. 3. With $\gamma_G = 0.017$ g/cm^3 d^{-1}, $\gamma_L = 1.98\times10^{-13}$ g/cm^3 d^{-1}, $\gamma_O = 1.46\times10^{-4}$ g/cm^3 d^{-1}, $\gamma_P = 1.83\times10^{-6}$ g/cm^3 d^{-1} and $\hat{\gamma}_P = 0$ for breakfast and lunch, and $\gamma_G = 2\times0.017$ g/cm^3 d^{-1}, $\gamma_L = 2\times1.98\times10^{-13}$ g/cm^3 d^{-1}, $\gamma_O = 2\times1.46\times10^{-4}$ g/cm^3 d^{-1}, $\gamma_P = 2\times1.83\times10^{-6}$ g/cm^3 d^{-1} and $\hat{\gamma}_P = 0$ for dinner. G and G_{24} in units of g/cm^3.

Obesity-induced diabetes

We assume that a person, who takes large amounts of food for a long time, gains weight and moves towards obesity, so that this person's adipose tissue is increasing, and so is the palmitic acid that is released from the adipose tissue. We represent this situation by increasing both the food function in Eq. (2.1) by a factor > 1, and the palmitic-acid release factor $\hat{\gamma}_P$.

In Fig. 7 we consider several levels of obesity by increasing food function in Eq. (2.1) by factors 2, 3, 4 and 4, and, correspondingly, multiplying $\hat{\gamma}_P$ by factors 1, 2, 3 and 4, respectively. We represent these factors, in the simulations, by multiplying the food parameters λ_G, λ_L, λ_O and λ_P by the time-dependent function f_λ, and by multiplying the parameters $\hat{\gamma}_P$, $2\hat{\gamma}_P$ and $4\hat{\gamma}_P$ by the time-dependent function f_γ, where:

$$f_\lambda(t;t_0,\text{Factor}) = 1 + (\text{Factor}-1)\frac{t}{t_0+t},$$
$$f_\gamma(t;t_0) = \frac{t}{t_0+t}; \tag{3.15}$$

we take $t_0 = 1$ year.

By the A1C test, we see that Patients #2 became prediabetic, Patient #3 remains prediabetic though progressed closer to diabetes, and Patients #4 and #5 became diabetic:

A1C test after 2 years :

$$\begin{cases} \text{Patient\#1} : \text{AVG}(G)|_{(\text{Factor}=1,\ 0\hat{\gamma}_P)} = 0.86 : \text{ Normal Healthy,} \\ \text{Patient\#2} : \text{AVG}(G)|_{(\text{Factor}=2,\ 1\hat{\gamma}_P)} = 1.22 : \text{ Prediabetic,} \\ \text{Patient\#3} : \text{AVG}(G)|_{(\text{Factor}=3,\ 2\hat{\gamma}_P)} = 1.36 : \text{ Prediabetic,} \\ \text{Patient\#4} : \text{AVG}(G)|_{(\text{Factor}=4,\ 3\hat{\gamma}_P)} = 1.43 : \text{ Diabetic,} \\ \text{Patient\#5} : \text{AVG}(G)|_{(\text{Factor}=4,\ 4\hat{\gamma}_P)} = 1.52 : \text{ Diabetic.} \end{cases} \tag{3.16}$$

With the same eating habits, the accumulation of adipose tissue may vary from one person to another. If, for instance, Patient #5 accumulated less adipose tissue over the 2 years so that the release of suppressed palmitic acid is at a level of $3\hat{\gamma}_P$, then AVG(G) = 1.43 g/cm^3; this is a case of diabetes. But with a factor of only $2.6\hat{\gamma}_P$ (simulations not shown here), it is a prediabetic case.

4. Drugs treatment of diabetes type 2

Mounjaro and Ozempic are recently approved drugs for treatment in diabetes. Each of these drugs increases insulin secretion through activating GLP-1 by GLP-1 receptor agonist; they also lower glucagon level (Lilly, 2023a,b; novoMEDLINK, 2023; Anderson, 2023). Both

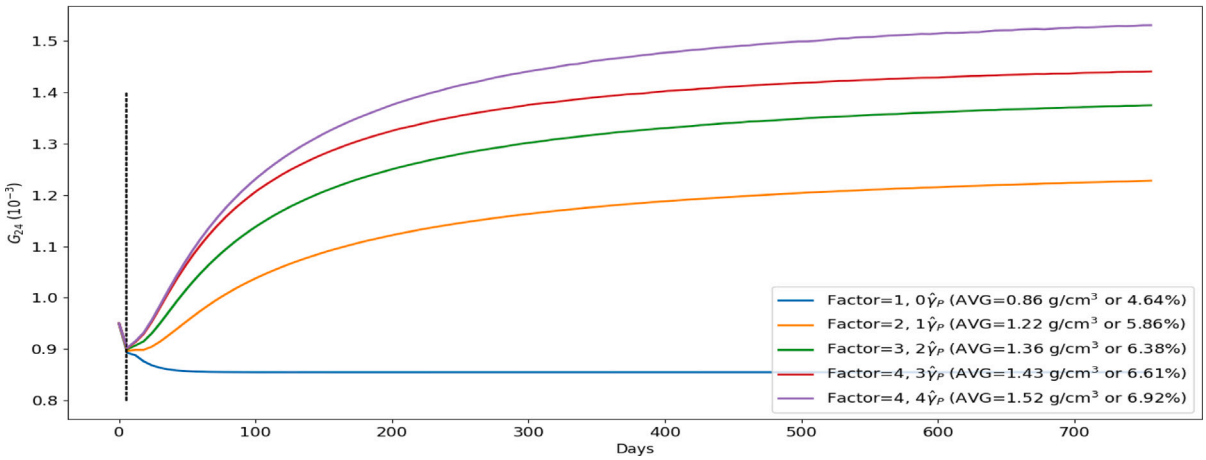

Fig. 7. Two years, 3 meals per day: 24-h glucose level for individuals with different feeding habits; "Factor=1, 0$\hat{\gamma}_P$" is equivalent to the food intake in Fig. 6. 'AVG' is the average glucose level over the last 3 months of the 2-year control period (the vertical dashed line represents day 5). The baselines are as follows: $\gamma_G = 0.017$ g/cm^3 d^{-1}, $\gamma_L = 1.98\times10^{-13}$ g/cm^3 d^{-1}, $\gamma_O = 1.46\times10^{-4}$ g/cm^3 d^{-1} and $\gamma_P = 1.83\times10^{-6}$ g/cm^3 d^{-1} for breakfast and lunch, and $\gamma_G = 2\times0.017$ g/cm^3 d^{-1}, $\gamma_L = 2\times1.98\times10^{-13}$ g/cm^3 d^{-1}, $\gamma_O = 2\times1.46\times10^{-4}$ g/cm^3 d^{-1} and $\gamma_P = 2\times1.83\times10^{-6}$ g/cm^3 d^{-1} for dinner; $\hat{\gamma}_P = 5.72\times10^{-5}$ g/cm^3 d^{-1}. G_{24} in units of g/cm^3.

drugs slow gastric emptying, that is, they slow down fast food travel through the digestive system, which makes the patient feel satisfied with a smaller amount of food, and results in weight loss.

Our model does not distinguish between these two drugs. So, for definiteness, we consider treatment with Mounjaro. Dosing schedule is weekly injection of 2.5 mg for the first 4 weeks and 5 mg for the following week. Denoting the drug by D, we represent the effect of D by rewriting Eqs. (2.2) and (2.9) as follows:

$$\frac{dL}{dt} = \lambda_L(t)(1+\frac{D}{K_D+D}) - \mu_{LB}BL - \mu_{LA}AL, \tag{4.17}$$

$$\frac{dG}{dt} = \frac{\lambda_G(t)}{1+D/\hat{K}_D} - \lambda_{G^*}(t)G + \lambda_{G^*U_2}G^*\frac{U_2}{K_{U_2}+U_2} - \lambda_{GU_4}G\frac{U_4}{K_{U_4}+U_4}, \tag{4.18}$$

with $\mu_{GD} > 0$.

Treatment with mounjaro

Clinical trials studying Mounjaro for weight loss found that participants lost an average of 12%–22% of their body weight over 68 weeks when using a high dose of the drug (10–15 mg) along with diet and exercise (Outlook India, 2023). In other studies of glycemic control with primary endpoint at 40 or 52 weeks, mean reductions in A1C, with baseline 7.9–8.6%, ranged between 1.8–2.1% with the 5 mg dose of Mounjaro, 1.7–2.4% with the 10 mg dose, and 1.7–2.4% with the 15 mg dose (Lilly, 2023c).

We start treatment with Patient #5 at $t = t_0 = 1$ year, when the patient has been diabetic already for several months.

We decrease the patient's food factor gradually by multiplying it by $\left(1-\frac{t-t_0}{K_1+(t-t_0)}\right)$, $t_0 = 365$ days, $t_0 < t < 730$, and take $1-\frac{365}{K_1+365} = 0.85$, or equivalently $K_1 = 2068$ days.

This means that the patient's food intake has been reduced by 15% in one year treatment, and, presumably this was accompanied by a weight loss of somewhat less than 15%, which is in the range seen in patients treated with Mounjaro (Lilly, 2023c). Since the patient's adipose tissue has correspondingly decreased, we multiply $\hat{\gamma}_P$ by $1-\frac{t-t_0}{K_2+(t-t_0)}$, $t_0 < t < 730$, where $K_2 = 2068$ days.

In Fig. 8, we simulated different cases of treatment of Patient #5 with Mounjaro; for clarity, we included both the glucose level ('AVG' in units of g/cm^3) and the A1C test result in 'percent'. When we started treating Patient #5 at Year 1, the A1C test result was 6.82%: a case of severe diabetes. After treating the patient for 1 year. A1C was reduced to 6.51% in Case 1 ($D = 0.5\times10^{-7}$ g/cm^3), 6.38% in Case 2 ($D = 10^{-7}$ g/cm^3) and 6.23% in Case 3 ($D = 1.5\times10^{-7}$ g/cm^3); patients in Cases 2 and 3 become prediabetic, while in Case 3 the patient remained diabetic but the level of A1C was significantly decreased.

In Fig. 9, following experiments in Lilly (2023c), we simulated different cases of treatment of

Patient #6: Factor=5, 9$\hat{\gamma}_P$,

whose feeding habits resulted in a more severe case of obesity-induced diabetes than the previous patients (Patients #1 to #5). We treated Patient #6 for 1 year in the same way as in Fig. 8, and obtained reductions in the A1C test results from 8.23% to 6.63% in Case 1, to 6.49% in Case 2, and to 6.24% in Case 3, in agreement with results reported in Lilly (2023c).

Treatment with Ozempic can be simulated in the same way as with Mounjaro, since both drugs activate GLP-1 and lower glucagon level. There are, of course, other drugs, like metformin, that are used to treat diabetes, but they do not report significant reduction in weight MedlinePlus (2023).

5. Conclusion

Obesity is a major driver of T2DM: 85% of adult Americans with T2DM are overweight or obese, and 30% of obese adults have the disease. Studies have identified causes and mechanisms which make obesity a high risk for T2DM (Zaki et al., 2020). In this paper, we developed a mathematical model that explains how obesity is likely to lead to T2DM and used the model to evaluate the efficacy of anti-T2DM drugs for obese patients.

The dominant paradigm for modeling the obesity-induced T2DM today focuses on glucose and insulin regulatory systems, diabetes pathways, and diagnostic test evaluations (Palumbo et al., 2013). As a result, most mathematical models tend to emulate the pathophysiology of glucose metabolism in T2DM in the blood. The problem with this approach is that it is not possible to explicitly account for the glucose transport mechanism from the blood to the liver, where the glucose is stored, and then from the liver to the blood. This makes it inaccurate, if not incorrect, to properly model the concentration of glucose in the blood in comparison to actual glycated hemoglobin (A1C) test results.

In order to understand how obesity affects glucose level in the blood and increases the risk of T2DM, we start the model with GLP-1, a hormone that increases in response to food intake; GLP-1 induces pancreatic β-cells to secrete insulin. We include in the model two transport proteins, GLUT-4 and GLUT-2. When GLUT-4 is activated

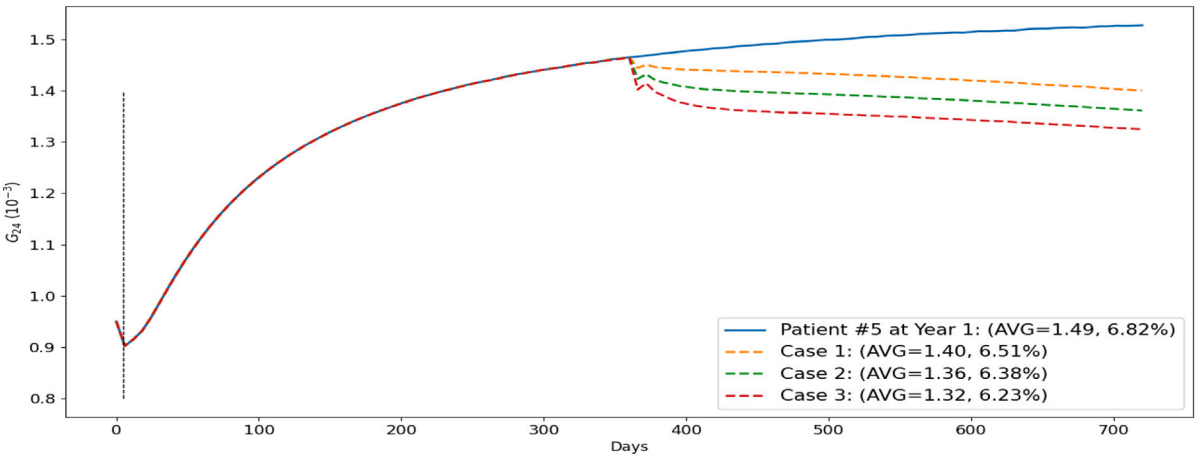

Fig. 8. Treatment with Mounjaro: The continuous curve is the same as for Patient #5 in Fig. 7 and the dashed curves show the results of the treatments with Mounjaro at different dose levels D. Treatment starts after 1 year (the profiles in Fig. 7). Case 1: $D = 0.5 \times 10^{-7}$ g/cm^3; Case 2: $D = 10^{-7}$ g/cm^3; Case 3: $D = 1.5 \times 10^{-7}$ g/cm^3. G_{24} in units of g/cm^3.

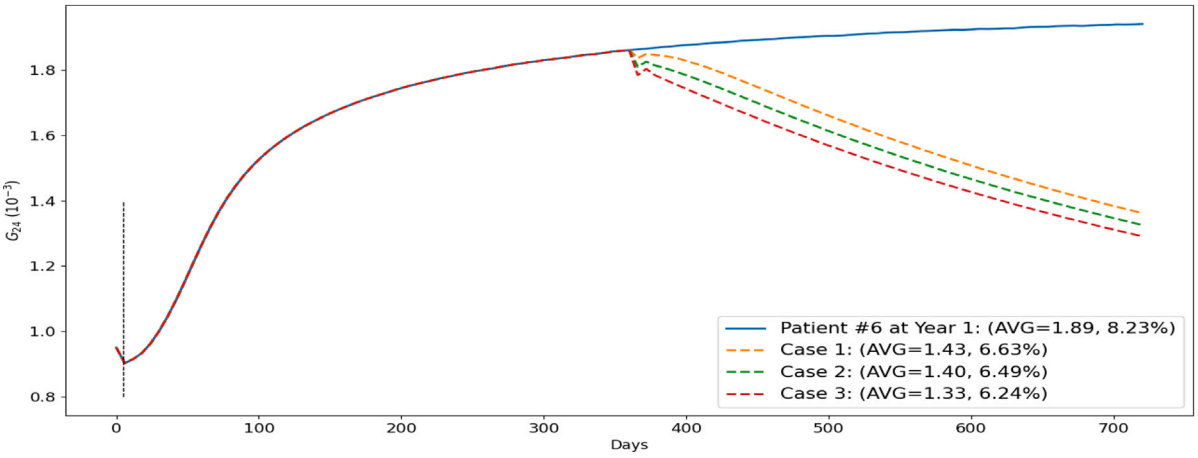

Fig. 9. Treatment with Mounjaro: The continuous curve is for the untreated Patient #6, and the dashed curves show the results of treatment with Mounjaro at different dose levels D. Treatment starts after 1 year. Case 1: $D = 0.5 \times 10^{-7}$ g/cm^3; Case 2: $D = 10^{-7}$ g/cm^3; Case 3: $D = 1.5 \times 10^{-7}$ g/cm^3. G_{24} in units of g/cm^3.

by insulin, it transports glucose from the blood to the liver, where it is stored in a non-toxic form, as glycogen. GLUT-2 is activated by pancreatic α-cells when blood glucose is low, and it transports the 'liver glucose' (glycogen), as glucose to the blood.

A state of obesity results from eating abnormally large amounts of food, thus accumulating adipose tissue, which stores pro-inflammatory acids, such as palmitic acid. The risk of T2DM arises from the inflammation released from the stored adipose, especially during a meal (Jelic et al., 2009; Virtamen, 2019; Carta et al., 2017; Oh et al., 2018).

We simulated the model with virtual healthy persons that became obese over a period of 2 years and used A1C test to show that some became prediabetic while others became diabetic.

These results suggest that a treatment of obese and diabetic individual with a drug that is both anti-diabetic and weight reducing could be significantly effective in decreasing the diabetic severity. To confirm this suggestion, we demonstrated that treatment, for one year of a virtual obese patient, decreased the severity of diabetes, and, at some dose levels, the patient became prediabetic; furthermore, the weight loss, in the simulations, was in agreement with data (Lilly, 2023c). Ozempic is another weight reducing, anti-T2DM drugs, and treatment with ozempic yields similar results.

The mathematical model uses some simplifying assumptions; due to the lack of data, we took some coefficients that should depend on time, especially during a meal, to be constant, and chose the constants to get agreement with data about average concentrations of glucose and insulin after a meal. We also took the effect of the drug to be a constant parameter. In another simplifying assumption, we did not go into details of the process of glucose/glycogen exchange inside the liver.

The mathematical model developed in this paper can be used to test and assess new experimental or approved T2DM drugs for obese diabetic patients.

6. Parameter sensitivity analysis

We performed sensitivity analysis with respect to the 24-h average glucose concentration Day 35, $G_{24}(35)$, for a non-obese and non-diabetic individual (without drugs), for the transition/activation parameters λ_L, λ_A, λ_B, λ_{IB}, λ_{CA}, λ_{U_2C}, λ_{U_4I}, λ_G, λ_{G^*}, λ_{GU_4}, $\lambda_{G^*U_2}$, λ_{T_α}, $\lambda_{T_\alpha P}$, λ_O, λ_P, γ_1, γ_2 and η_{T_α}.

The computations were done using Latin Hypercube Sampling/Partial Rank Correlation Coefficient (LHS/PRCC) with a Matlab package by Kirschner (2007–2008), Marino et al. (2008). The range for the parameters in the sensitivity analysis was between ±50% of their baseline values in Table 2.

Expectedly, increasing the baseline secretion rate of glucose, λ_G, results in the highest increase in $G_{24}(35)$, and increasing the baseline early glucose elimination rate of glucose, λ_{G^*}, results in the most decrease in $G_{24}(35)$.

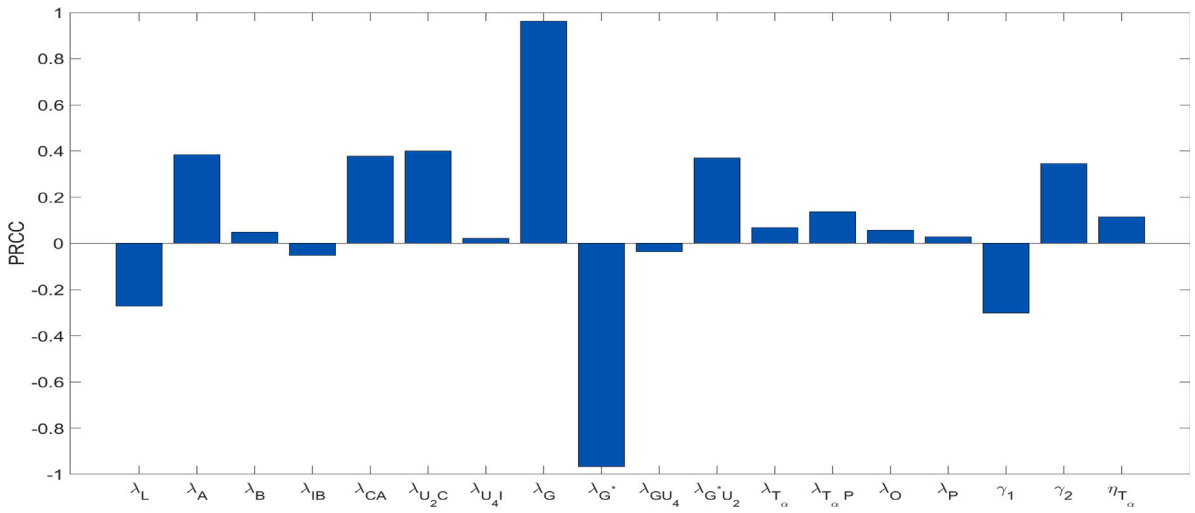

Fig. 10. Parameter sensitivity analysis for the 24-h average glucose concentration after 35 days. The p-values are less than 0.01.

Increasing the activation rate of α-cells, $\tilde{\lambda}_A$, results in a cascade of activities, including increased secretion (at rate λ_{CA}) and induction (at rate γ_2) of glucagon. Glucagon, in turn, stimulates GLUT-2 secretion, and GLUT-2 transports glucose from the liver to the blood at a rate $\lambda_{G^*U_2}$. Hence, the parameters $\tilde{\lambda}_A$, λ_{CA}, $\lambda_{G^*U_2}$, and γ_2 are positively correlated, while γ_1 and λ_{GU_4} are negatively correlated (see Fig. 10).

Decreased activity of GLUT-4 reduces the transport of glucose from the blood to the liver. Since increasing the secretion of TNF-α at rates λ_{T_α} and $\lambda_{T_\alpha P}$ leads to an increased deactivation of GLUT-4, λ_{T_α} and $\lambda_{T_\alpha P}$ are positively correlated.

If the transport rate of glucose by GLUT-4, λ_{GU_4}, increases, then glucose in the blood decreases as it is transported into the liver for storage. Consequently, λ_{GU_4} is negatively correlated with blood glucose levels.

7. Parameter estimations

Half-saturation

We denote by Z^0 the average density/concentration of species Z. In an expression of the form $Y\frac{X}{K_X+X}$ where Y is activated by X and the parameter K_X is the half-saturation of X, we assume that

$$\frac{X^0}{K_X+X^0}$$

to be not too close to 0 or to 1, and, for simplicity, take it to be 1/2, so that

$$K_X = X^0.$$

Estimate for L^0

In humans, fasting systemic plasma concentrations of GLP-1 are typically in the range of 5–10 pmol/L and it can increase up to 40 pmol/L in response to a meal (Orskov et al., 1996; Holst, 2007). We take 8 pmol/L when fasting, and 30 pmol/L after a meal. Since 1 mol/L= 5.56×10^{-4} g/cm^3, we get

$$L^0_{\text{fasting}} = 4.5\times10^{-15}\ \text{g/cm}^3, \quad L^0_{\text{meal}} = 1.67\times10^{-14}\ \text{g/cm}^3,$$

We take

$$K_L = 1.7\times10^{-14}\ \text{g/cm}^3, \quad \hat{K}_L = 1.7\times10^{-14}\ \text{g/cm}^3.$$

Estimates for G^0

Pancreatic insulin keeps the blood sugar in the range 60–100 mg/dL when fasting, and up to 140 mg/dL after meals (Kennedy et al., 2007–2022). We take 80 mg/dL when fasting, and 130 mg/dL after meals. Hence

$$G^0_{\text{fasting}} = 8\times10^{-4}\ \text{g/cm}^3, \quad G^0_{\text{meal}} = 1.3\times10^{-3}\ \text{g/cm}^3.$$

Estimates for P and O

Plasma concentrations in healthy humans (non-diabetic and nonobese) ranges between $0.3-4.1$ mmol/l for palmitic acid and $0.03-3.2$ mmol/l for oleic acid (Abdelmagid et al., 2015); we take 2.2 mmol/l (or equivalently, 1.22×10^{-6} g/cm^3 in healthy humans) for palmitic acid and 1.62 mmol/l (or equivalently, 6.78×10^{-7} g/cm^3 in healthy humans) for oleic acid.

The palmitic acid in high-fat diet (obese) mice was measured in Qiu et al. (2022)(Fig. 4 g) to be approximately twice that of non-obese mice; we take this ratio to be the same for oleic acid. We get

$$P^h \equiv P_{\text{health}} = 1.22\times10^{-6}\ \text{g/cm}^3 \text{ and } O^h \equiv O_{\text{health}} = 6.78\times10^{-7}\ \text{g/cm}^3;$$

$$P^o \equiv P_{\text{obese}} = 2.44\times10^{-6}\ \text{g/cm}^3 \text{ and } O^o \equiv O_{\text{obese}} = 1.36\times10^{-6}\ \text{g/cm}^3.$$

We take

$$\hat{K}_O = O_{\text{obese}} = 1.36\times10^{-6}\ \text{g/cm}^3.$$

Estimates for K_{U_2}, K_{U_4}, U_2^0 and U_4^0

The half-saturation of GLUT-4 is approximately 5 mmol/L (Gorovits and Charron, 2003) and that of GLUT-2 ranges in 15–20 mmol/L (Wolfsdorf and Weinstein, 2012). Since 1 mol/L= 5.56×10^{-4} g/cm^3, we get

$$K_{U_2} = 9.45\times10^{-6}\ \text{g/cm}^3, \quad K_{U_4} = 2.78\times10^{-6}\ \text{g/cm}^3.$$

We take

$$U_2^0 = 9.45\times10^{-6}\ \text{g/cm}^3, \quad U_4^0 = 2.78\times10^{-6}\ \text{g/cm}^3.$$

Estimate for I^0

We take

$$I_{\text{hypo}} = I^0_{\text{min}} = 0.9\times10^{-13}\ \text{g/cm}^3, \quad I^0_{\text{max}} = 10.7\times10^{-13}\ \text{g/cm}^3.$$

We also take

$$K_I = 2\times10^{-13}\ \text{g/cm}^3.$$

Estimate for C^0

The ratio of pancreatic glucagon concentration to insulin concentration is $C/I \approx 0.12$ for non-diabetic subjects and $C/I \approx 0.18$ for type 2 diabetic subjects (Henquin et al., 2017)(Fig 4 A). Hence, in the no-diabetes case we get:

$$C^0_{\text{fasting}} = 5.4\times 10^{-16}\ \text{g/cm}^3, \quad C^0_{\text{meal}} = 20\times 10^{-16}\ \text{g/cm}^3$$

Estimate for T^0_α

T2DM is not an inflammatory disease, and the level of TNF-α for non-obese persons, which is approximately 6 pg/ml (Li et al., 2018), increases approximately to just 7 pg/ml (Alzamil, 2020). However, in obesity, the TNF-α increases several folds (Stanley et al., 2011), and this inflammation may lead to diabetes 2.

The level of TNF-α is almost the same in non-obese (diabetic or not) persons, at $T_\alpha \simeq 7$ pg/ml; in obese persons, $T_\alpha \simeq 8$ pg/ml in diabetic patients and $T_\alpha \simeq 6$ pg/ml in non-diabetic persons (Alzamil, 2020). We take

$T^0_\alpha = 7\times 10^{-12}$ g/cm^3 in non-obese persons,

$T^0_\alpha = 8\times 10^{-12}$ g/cm^3 in obese diabetic patients and

$T^0_\alpha = 6\times 10^{-12}$ g/cm^3 in obese non-diabetic persons

Decay, degradation and deactivation rates

Estimates for μ_{LB} and μ_{LA}

The half-lifeof GLP-1 is approximately 2 min (Sharma et al., 2018). We take the elimination rate of GLP-1 by B and A to be

$$\mu_{LB} = 251\ \text{cm}^3/\text{g d}^{-1} \quad \text{and} \quad \mu_{LA} = 251\ \text{cm}^3/\text{g d}^{-1}.$$

Estimate for μ_A and μ_B

The half-life of β-cells in young rodents is 30–60 days (Jones et al., 2015; Cerf, 2013; Finegood et al., 1995). However, β-cells become activated during a part of a day, and then are deactivated (hours after a meal). Hence the half-life of activation to deactivation is a few hours. We take $t_B^{1/2} = 2$ hours (0.083 days) and get

$$\mu_B = \frac{\ln 2}{0.083\ \text{d}} = 8.32\ \text{d}^{-1}.$$

We take

$$\mu_A = 8.32\ \text{d}^{-1}.$$

Estimate for μ_I

The plasma half-life of insulin ranges between 4–6 min Morishima et al. (1992), Duckworth (1988); we take 5 min (3.5×10^{-3} d). Hence,

$$\mu_I = \frac{\ln 2}{3.5\times 10^{-3}\ \text{d}} = 198.04\ \text{d}^{-1}.$$

Estimate for μ_{U_4}

The half-life of GLUT-4 ranges in 8–10 h (Host et al., 1998; Schnurr et al., 2015); we take 9 h (0.375 d). Hence,

$$\mu_{U_4} = \frac{\ln 2}{0.375\ \text{d}} = 1.85\ \text{d}^{-1}.$$

Estimate for μ_{U_2}

The half-life of GLUT-2 is 3.5 h (0.15 d) (Hou et al., 2009). Hence,

$$\mu_{U_2} = \frac{\ln 2}{0.15\ \text{d}} = 4.62\ \text{d}^{-1}.$$

Estimate for μ_C

The half-life of glucagon 6–7 min (Norman and Litwack, 1997); we take 6 min (4.17×10^{-3} d). Hence,

$$\mu_C = \frac{\ln 2}{4.17\times 10^{-3}\ \text{d}} = 166.22\ \text{d}^{-1}.$$

Estimate for μ_D

The half-life of tirzepatide (brand name for Mounjaro) is approximately 5 days (Lilly, 2022). Hence,

$$\mu_D = \frac{\ln 2}{5\ \text{d}} = 0.139\ \text{d}^{-1}.$$

Estimates for $\lambda_G(t)$ and $\lambda_{G^*}(t)$

We take $\lambda_G(t) = \gamma_G$ if $0 \le t \le 1$, and $\lambda_G(t) = 0$ if $t > 1$, where

$\gamma_G = 0.017$ g/cm^{3}d^{-1}.

We also take $\lambda_{G^*}(t) = \gamma_{G^*}$ if $1 \le t \le 3$, and $\lambda_{G^*}(t) = 0$ if $t < 1$ or $t > 3$, where

$$\gamma_{G^*} = 11.1\ \text{d}^{-1}.$$

Estimates for γ_O, γ_P, μ_O and μ_P

The effective rate constants for the oxidative degradation of oleic acid in atmospheric conditions range in between 0.08–0.57 hr^{-1} (Li et al., 2023). We assume this rate in blood plasma to be large and take $\mu_O = 0.57$ hr^{-1}, or equivalently

$$\mu_O = 13.68\ \text{d}^{-1}.$$

Since oleic acid degrades faster than palmitic acid (Nabors et al., 1984), we take

$$\mu_P = 12\ \text{d}^{-1}.$$

We take

$$\gamma_O = 1.46\times 10^{-4}\ \text{g/cm}^3\ \text{d}^{-1} \quad \text{and} \quad \gamma_P = 1.83\times 10^{-6}\ \text{g/cm}^3\ \text{d}^{-1}.$$

Eq. (2.12)

We take,

$$\lambda_{T_\alpha} = 1.19\times 10^{-9}\ \text{g/cm}^3\ \text{d}^{-1} \quad \text{and} \quad \lambda_{T_\alpha P} = 3.26\times 10^{-4}\ \text{d}^{-1}$$

so that, in steady state,

$$T_\alpha = \frac{\lambda_{T_\alpha} + \lambda_{T_\alpha P} P^0/2}{\mu_{T_\alpha}} = T^0_\alpha$$

where $\mu_{T_\alpha} = 199\ \text{d}^{-1}$ (Simo et al., 2012; Siewe and Friedman, 2020), $P = P^0 = 2.44\times 10^{-6}$ g/cm^3, $T^0_\alpha = 6\times 10^{-12}$ g/cm^3 is the steady state in obese and non-diabetic case.

Declaration of competing interest

The authors declare that they have no known competing financial interests or personal relationships that could have appeared to influence the work reported in this paper.

Acknowledgment

The first author was supported by the School of Mathematics and Statistics at Rochester Institute of Technology, USA.

References

Abdelmagid, S.A., Clarke, S.E., Nielsen, D.E., Badawi, A., El-Sohemy, A., Mutch, D.M., et al., 2015. Comprehensive profiling of plasma fatty acid concentrations in young healthy Canadian adults. PLoS One 10 (2), e0116195. http://dx.doi.org/10.1371/journal.pone.0116195.

Agrawal, S., Makuch, S., Drozdz, M., Dudzik, T., Domanski, I., Poreba, R., et al., 2022. The impact of hypoglycemia on patients with diabetes mellitus: A cross-sectional analysis. J. Clin. Med. 11 (3), 626. http://dx.doi.org/10.3390/jcm11030626.

Alzamil, H., 2020. Elevated serum TNF-α is related to obesity in type 2 diabetes mellitus and is associated with glycemic control and insulin resistance. J. Obesity. 2020 (5076858), 1–5. http://dx.doi.org/10.1155/2020/5076858.

American Diabetes Association, 2022. eAG/A1C conversion calculator. DiabetesPro. https://professional.diabetes.org/diapro/glucose_calc.

Anderson, L.A., 2023. Mounjaro vs Ozempic: How do they compare?. https://www.drugs.com/medical-answers/mounjaro-ozempic-compare-3571637/. (Accessed 4 July 2023).

BD Editors, 2017. Glycogenolysis. Biological Dictionary: https://biologydictionarynet/glycogenolysis/.

Boutayeb, W., Lamlili, M.E.N., Boutayeb, A., Derouich, M., 2015. The impact of obesity on predisposed people to type 2 diabetes: Mathematical model. In: Ortuño, F., Rojas, I. (Eds.), Bioinformatics and Biomedical Engineering IWBBIO. p. 9043. http://dx.doi.org/10.1007/978-3-319-16483-0_59.

Buppajarntham, S., Junpaparp, P., Salameh, R., Anastasopoulou, C., Staros, E.B., 2021. Insulin. Medscape. https://emedicine.medscape.com/article/2089224--overview?reg=1.

Butler, P.C., Meier, J.J., Butler, A.E., Bhushan, A., 2007. The replication of beta cells in normal physiology, in disease and for therapy. Nat. Clin. Pract. Endocrinol. Metab. 3 (11), 758–768. http://dx.doi.org/10.1038/ncpendmet0647.

Carta, G., Murru, E., Banni, S., Manca, C., 2017. Palmitic acid: Physiological role, metabolism and nutritional implications. Front. Physiol. 8 (902), http://dx.doi.org/10.3389/fphys.2017.00902.

Castoldi, A., Naffah de Souza, C., Câmara, N.O., Moraes-Vieira, P.M., 2016. The macrophage switch in obesity development. Front Immunol. 6 (637), http://dx.doi.org/10.3389/fimmu.2015.00637.

Castro, M.R., 2022. GLP-1 Agonists: Diabetes Drugs and Weight Loss. Mayo Clinic.

CDC, 2022. All About Your, A1C. Centers for Disease Control and Prevention, www.cdc.gov/diabetes/managing/managing-blood-sugar/.

Cerf, M.E., 2013. Beta cell dysfunction and insulin resistance. Front. Endocrinol. (Lausanne) 4 (37), http://dx.doi.org/10.3389/fendo.2013.00037.

Chandra, K., Jain, V., Jain, S.K., 2021. Plasma non-esterified fatty acids (NEFA) in type 2 diabetes mellitus: Evidence on pathophysiology. J. Diabetes Clin. Res. 3 (2), 46–50.

Chen, X.M., Zhang, W.Q., Tian, Y., Wang, L.F., Chen, C.C., Qiu, C.M., 2018. Liraglutide suppresses non-esterified free fatty acids and soluble vascular cell adhesion molecule-1 compared with metformin in patients with recent-onset type 2 diabetes. Cardiovasc. Diabetol. 17 (1), 53. http://dx.doi.org/10.1186/s12933-018-0701-4.

Cnop, M., Welsh, N., Jonas, J.C., Jörns, A., Lenzen, S., Eizirik, D.L., 2005. Mechanisms of pancreatic beta-cell death in type 1 and type 2 diabetes: many differences, few similarities. Diabetes 54 (Suppl 2), S97–S107. http://dx.doi.org/10.2337/diabetes.54.suppl_2.s97.

Cohen, P., Nimmo, H.G., Proud, C.G., 1978. How does insulin stimulate glycogen synthesis? Biochem. Soc. Symp. 43, 69–95.

da Costa, R.M., Neves, K.B., Mestriner, F.L., Louzada-Junior, P., Bruder-Nascimento, T., Tostes, R.C., 2016. TNF-α induces vascular insulin resistance via positive modulation of PTEN and decreased Akt/eNOS/NO signaling in high fat diet-fed mice. Cardiovasc. Diabetol. 15 (1), 119. http://dx.doi.org/10.1186/s12933-016-0443-0.

Drucker, D.J., 2018. Mechanisms of action and therapeutic application of glucagon-like peptide-1. Cell Metab. 27 (4), 740–756. http://dx.doi.org/10.1016/j.cmet.2018.03.001.

Duckworth, W.C., 1988. Insulin degradation: mechanisms, products, and significance. Endocr. Rev. 9 (3), 319–345. http://dx.doi.org/10.1210/edrv-9-3-319.

El Bacha, T., Luz, M., Da Poian, A., 2010. Dynamic adaptation of nutrient utilization in humans. Nat. Educ. 3 (9), 8.

Finegood, D.T., Scaglia, L., Bonner-Weir, S., 1995. Dynamics of beta-cell mass in the growing rat pancreas, Estimation with a simple mathematical model. Diabetes 44, 249–256. http://dx.doi.org/10.2337/diab.44.3.249.

Fraser, D.A., Thoen, J., Rustan, A.C., Forre, O., Kjeldsen-Kragh, J., 1999. Changes in plasma free fatty acid concentrations in rheumatoid arthritis patients during fasting and their effects upon T-lymphocyte proliferation. Rheumatology (Oxford) 38 (10), 948–952. http://dx.doi.org/10.1093/rheumatology/38.10.948.

Frayn, K.N., 1998. Non-esterified fatty acid metabolism and postprandial lipaemia. Atherosclerosis 141 (Suppl 1), S41–6. http://dx.doi.org/10.1016/s0021-9150(98)00216-0.

Gorovits, N., Charron, M.J., 2003. What we know about facilitative glucose transporters: Lessons from cultured cells, animal models, and human studies. Biochem. Mol. Biol. Educ. 31 (3), 163–172. http://dx.doi.org/10.1002/bmb.2003.494031030227.

Green, C.J., Henriksen, T.I., Pedersen, B.K., Solomon, T.P., 2012. Glucagon like peptide-1-induced glucose metabolism in differentiated human muscle satellite cells is attenuated by hyperglycemia. PLoS One 7 (8), e44284. http://dx.doi.org/10.1371/journal.pone.0044284.

Gupta, A., 2022. Direct and indirect actions of insulin: role of insulin receptor, glucose transporters (GLUTs), and sodium-glucose linked transporters (SGLTs). Underst. Insulin Insulin Resist. 6, 179–201. http://dx.doi.org/10.1016/B978-0-12-820234-0.00003-2.

Hampton, G.S., Bartlette, K., Nadeau, K.J., Cree-Green, M., Behn, C.D., 2022. Mathematical modeling reveals differential dynamics of insulin action models on glycerol and glucose in adolescent girls with obesity. Front. Physiol. 13 (895118), http://dx.doi.org/10.3389/fphys.2022.895118.

Henquin, J.C., Ibrahim, M.M., Rahier, J., 2017. Insulin, glucagon and somatostatin stores in the pancreas of subjects with type-2 diabetes and their lean and obese non-diabetic controls. Sci. Rep. 7 (1), 11015. http://dx.doi.org/10.1038/s41598-017-10296-z.

Heskey, C.E., Jaceldo-Siegl, K., Sabaté, J., Fraser, G., Rajaram, S., 2016. Adipose tissue α-linolenic acid is inversely associated with insulin resistance in adults. Am. J. Clin. Nutr. 103 (4), 1105–1110. http://dx.doi.org/10.3945/ajcn.115.118935.

Holst, J., 2007. The physiology of glucagon-like peptide 1. Physiol. Rev. 87 (4), 1409–1439. http://dx.doi.org/10.1152/physrev.00034.2006.

Hosokawa, M., Thorens, B., 2002. Glucose release from GLUT2-null hepatocytes: characterization of a major and a minor pathway. Am. J. Physiol. Endocrinol. Metab. 282 (4), E794–801. http://dx.doi.org/10.1152/ajpendo.00374.2001.

Host, H.H., Hansen, P.A., Nolte, L.A., Chen, M.M., Holloszy, J.O., 1998. Rapid reversal of adaptive increases in muscle GLUT-4 and glucose transport capacity after training cessation. J. Appl. Physiol. (1985) 84 (3), 798–802. http://dx.doi.org/10.1152/jappl.1998.84.3.798.

Hou, J.C., Williams, D., Vicogne, J., J.E., Pessin, 2009. The glucose transporter 2 undergoes plasma membrane endocytosis and lysosomal degradation in a secretagogue-dependent manner. Endocrinol. 150 (9), 4056–4064. http://dx.doi.org/10.1210/en.2008-1685.

Huang, J., Takeshi, I., Olefsky, J.M., 2001. Insulin can regulate GLUT4 internalization by signaling to Rab5 and the motor protein dynein. Proc. Natl. Acad. Sci. USA 98 (23), 13084–13089, www.jstor.org/stable/3057044.

Jacobson, D.A., Wicksteed, B.L., Philipson, L.H., 2009. The alpha-cell conundrum: ATP-sensitive K+ channels and glucose sensing. Diabetes 58 (2), 304–306. http://dx.doi.org/10.2337/db08-1618.

Jelic, K., Hallgreen, C.E., Colding-Jørgensen, M., 2009. A model of NEFA dynamics with focus on the postprandial state. Ann. Biomed. Eng. 37 (9), 1897–1909. http://dx.doi.org/10.1007/s10439-009-9738-6.

Jensen, J., Rustad, P.I., Kolnes, A.J., Lai, Y.C., 2011. The role of skeletal muscle glycogen breakdown for regulation of insulin sensitivity by exercise. Front. Physiol. 2 (112), http://dx.doi.org/10.3389/fphys.2011.00112.

Jones, D.D., Wilmore, J.R., Allman, D., 2015. Cellular dynamics of memory B cell populations: IgM+ and IgG+ memory B cells persist indefinitely as quiescent cells. J. Immunol. 195 (10), 4753–4759. http://dx.doi.org/10.4049/jimmunol.1501365.

Kang, Z.F., Deng, Y., Zhou, Y., Fan, R.R., Chan, J.C., Laybutt, D.R., et al., 2013. Pharmacological reduction of NEFA restores the efficacy of incretin-based therapies through GLP-1 receptor signalling in the beta cell in mouse models of diabetes. Diabetologia 56 (2), 423–433. http://dx.doi.org/10.1007/s00125-012-2776-x.

Karpe, F., Dickmann, J.R., Frayn, K.N., 2011. Fatty acids, obesity, and insulin resistance: time for a reevaluation. Diabetes 60 (10), 2441–2449. http://dx.doi.org/10.2337/db11-0425.

Kawamori, D., 2017. Exploring the molecular mechanisms underlying α- and β-cell dysfunction in diabetes. Diabetol. Int. 8 (3), 248–256. http://dx.doi.org/10.1007/s13340-017-0327-x.

Kennedy, M.N., Bedrich, M., Gray, L.W., Kroon, L., Demetsky, M., 2007–2022. Insulin basics. Diabetes Education Online.

Kirschner, D.E., 2007–2008. Uncertainty and Sensitivity Functions and Implementation. University of Michigan, http://malthus.micro.med.umich.edu/lab/usadata/.

Klein, J., Dolzan, V., 2022. Glucagon-like peptide-1 receptor agonists in the management of type 2 diabetes mellitus and obesity: The impact of pharmacological properties and genetic factors. Int. J. Mol. Sci. 23 (7), 3451. http://dx.doi.org/10.3390/ijms23073451.

Knudsen, L.B., Lau, L., 2019. The discovery and development of liraglutide and semaglutide. Front. Endocrinol. (Lausanne) 10 (155), http://dx.doi.org/10.3389/fendo.2019.00155.

Lauterbach, M.A.R., Wunderlich, F.T., 2017. Macrophage function in obesity-induced inflammation and insulin resistance. Pflugers Arch. 469 (3–4), 385–396. http://dx.doi.org/10.1007/s00424-017-1955-5.

Li, G., Wu, W., Zhang, X., Huang, Y., Wen, Y., Li, X., et al., 2018. Serum levels of tumor necrosis factor alpha in patients with IgA nephropathy are closely associated with disease severity. BMC Nephrol. 19 (326), http://dx.doi.org/10.1186/s12882-018-1069-0.

Li, R., Zhang, K., Li, Q., Yang, L., Wang, S., Liu, Z., et al., 2023. Characteristics and degradation of organic aerosols from cooking sources based on hourly observations of organic molecular markers in urban environments. Atmos. Chem. Phys. 23, 3065–3081. http://dx.doi.org/10.5194/acp-23-3065-2023.

Lilly, E., 2022. Highlights of prescribing information: Mounjaro(TM) (tirzepatide) injection, for subcutaneous use initial U.S. Eli Lilly and Company (approval: 2022). Ref ID: 4983783.

Lilly, E., 2023a. Mounjaro (tirzepatide) for the Treatment of Type 2 Diabetes. Clin Trials Arena, USA, https://www.clinicaltrialsarena.com/projects/mounjaro-tirzepatide-type-2-diabetes/. (Accessed 4 July 2023).

Lilly, E., 2023b. One Weekly Mounjaro (tirzepatide) Injection. Eli Lilly and Company, https://www.mounjaro.com/hcp/how-mounjaro-works. (Accessed 4 July 2023).

Lilly, E., 2023c. Reset Your Expectations with Mounjaro. Eli Lilly and Company, https://www.mounjaro.com/hcp/a1c-weight#mounjaro-a1c. (Accessed July 4 2023).

López-Palau, N.E., Olais-Govea, J.M., 2020. Mathematical model of blood glucose dynamics by emulating the pathophysiology of glucose metabolism in type 2 diabetes mellitus. Sci. Rep. 10 (1), 12697. http://dx.doi.org/10.1038/s41598-020-69629-0.

Lu, H., Hao, L., Li, S., Lin, S., Lv, L., Chen, Y., et al., 2016. Elevated circulating stearic acid leads to a major lipotoxic effect on mouse pancreatic beta cells in hyperlipidaemia via a miR-34a-5p-mediated PERK/p53-dependent pathway. Diabetologia 59 (6), 1247–1257. http://dx.doi.org/10.1007/s00125-016-3900-0.

Lynch, E., Llano, A., 2023. Drugs used in the management of hyperglycaemia. Anaesth. Intensiv. Care Med. 24 (1), 78–81. http://dx.doi.org/10.1016/j.mpaic.2022.10.014.

Mari, A., Tura, A., Grespan, E., Bizzotto, R., 2020. Mathematical modeling for the physiological and clinical investigation of glucose homeostasis and diabetes. Front. Physiol. 11 (575789), http://dx.doi.org/10.3389/fphys.2020.575789.

Marino, S., Hogue, I.B., Ray, C.J., Kirschner, D.E., 2008. A methodology for performing global uncertainty and sensitivity analysis in systems biology. J. Theoret. Biol. 254, 178–196.

MedlinePlus, 2023. Metformin, MedlinePlus drug information. https://medlineplus.gov/druginfo/meds/a696005.html. (Access 4 July 2023).

Melmed, S., Polonsky, K.S., Larsen, P.R., Kronenberg, H.M., 2016. Williams Textbook of Endocrinology, 13th ed. Elsevier Saunders, Philadelphia.

Morishima, T., Pye, S., Bradshaw, C., Radziuk, J., 1992. Posthepatic rate of appearance of insulin: measurement and validation in the nonsteady state. Am. J. Physiol. 263 (4 Pt 1), E772–E779. http://dx.doi.org/10.1152/ajpendo.1992.263.4.E772.

Mukherjee, B., Hossain, C.M., Mondal, L., Paul, P., Ghosh, M.K., 2013. Obesity and insulin resistance: an abridged molecular correlation. Lipid Insights 6, 1–11. http://dx.doi.org/10.4137/LPI.S10805.

Nabors, L.A., Morgan, M.S., Newman, D.W., Jaworski, J.G., 1984. Preferential metabolism of linoleic acid by five-day-old barley shoots. Lipids. 19 (7), 507–514. http://dx.doi.org/10.1007/BF02534483.

Nani, F.K., Jin, M., 2015. Mathematical modeling and simulations of the pathophysiology of type-2 diabetes mellitus. Math and Computer Science Faculty Working Papers. http://digitalcommons.uncfsu.edu/macsc_wp/25.

Norman, A.W., Litwack, G., 1997. Pancreatic hormones: Insulin and glucagon. Hormones (2nd Ed.) 7, 193–227. http://dx.doi.org/10.1016/B978-012521441-4/50008-0.

novoMEDLINK, 2023. Important Safety Information for Ozempic (semaglutide) injection. Novo Nordisk, https://www.novomedlink.com/semaglutide.html#Ozempic-HCP-isi. (Accessed 4 July 2023).

Ogilvy-Stuart, A.L., Beardsall, K., 2020. Pathophysiology and management of disorders of carbohydrate metabolism and neonatal diabetes. Mat. Fetal Neonatal Endocrinol. 45, 783–803. http://dx.doi.org/10.1016/B978-0-12-814823-5.00046-5.

Oh, Y.S., Bae, G.D., Baek, D.J., Park, E.Y., Jun, H.S., 2018. Fatty acid-induced lipotoxicity in pancreatic beta-cells during development of type 2 diabetes. Front. Endocrinol. (Lausanne) 9 (384), http://dx.doi.org/10.3389/fendo.2018.00384.

Orskov, C., Wettergren, A., Holst, J.J., 1996. Secretion of the incretin hormones glucagon-like peptide-1 and gastric inhibitory polypeptide correlates with insulin secretion in normal man throughout the day. Scand. J. Gastroenterol. 31 (7), 665–670. http://dx.doi.org/10.3109/00365529609009147.

Ortuno, F., Rojas, I., 2015. Bioinformatics and biomedical engineering. In: Third International Conference, IWBBIO: Proceeding Part 1. In: LNBI 9043.

Outlook India, 2023. Mounjaro for weight loss reviews - mounjaro tirzepatide injection results for losing weight, cost and side effects. Outlook for Brands. https://www.outlookindia.com/outlook-spotlight/mounjaro-for-weight-loss-reviews-mounjaro-tirzepatide-injection-results-for-losing-weight-cost-and-side-effects-news-288692. (Accessed 7 July 2023).

Palumbo, P., Ditlevsen, S., Bertuzzi, A., De Gaetano, A., 2013. Mathematical modeling of the glucose-insulin system: a review. Math. Biosci. 244 (2), 69–81. http://dx.doi.org/10.1016/j.mbs.2013.05.006.

Patino, S.C., Orrick, J.A., 2023. Biochemistry, Glycogenesis. StatPearls, Treasure Island (FL), www.ncbi.nlm.nih.gov/books/NBK549820/.

Plomgaard, P., Bouzakri, K., Krogh-Madsen, R., Mittendorfer, B., Zierath, J.R., Pedersen, B.K., 2005. Tumor necrosis factor-α induces skeletal muscle insulin resistance in healthy human subjects via inhibition of Akt substrate 160 phosphorylation. Diabetes 54 (10), 2939–2945. http://dx.doi.org/10.2337/diabetes.54.10.2939.

Puddick, R., F., Moncrieff, Mounjaro, V.S., Ozempic, 2023. Second nature. https://www.secondnature.io/us/guides/lifestyle/mounjaro--vs--ozempic.

Qiu, T., Yang, X., Wang, J., Pan, C., Chu, X., Xiong, J., et al., 2022. Obesity-induced elevated palmitic acid promotes inflammation and glucose metabolism disorders through GPRs/NF-κB/KLF7 pathway. Nutr. Diabetes 12 (1), 23. http://dx.doi.org/10.1038/s41387-022-00202-6.

Rehni, A.K., Dave, K.R., 2018. Impact of hypoglycemia on brain metabolism during diabetes. Mol. Neurobiol. 55 (12), 9075–9088. http://dx.doi.org/10.1007/s12035-018-1044-6.

Richter, E.A., 2021. Is GLUT4 translocation the answer to exercise-stimulated muscle glucose uptake? Am. J. Physiol. Endocrinol. Metab. 320 (2), E240–E243. http://dx.doi.org/10.1152/ajpendo.00503.2020.

Riley, L., 2022. Mean Fasting Blood Glucose. World Health Organization, www.who.int/data/gho/indicator-metadata-registry/imr-details/2380.

Salvadó, L., Coll, T., Gómez-Foix, A.M., Salmerón, E., Barroso, E., Palomer, X., et al., 2013. Oleate prevents saturated-fatty-acid-induced ER stress, inflammation and insulin resistance in skeletal muscle cells through an AMPK-dependent mechanism. Diabetologia 56 (6), 1372–1382. http://dx.doi.org/10.1007/s00125-013-2867-3.

Samkani, A., Skytte, M.J., Anholm, C., Astrup, A., Deacon, C.F., Holst, J.J., et al., 2018. The acute effects of dietary carbohydrate reduction on postprandial responses of non-esterified fatty acids and triglycerides: a randomized trial. Lipids Health Dis. 17 (1), 295. http://dx.doi.org/10.1186/s12944-018-0953-8.

Schnurr, T.M., Reynolds, A.J., Komac, A.M., Duffy, L.K., Dunlap, K.L., 2015. The effect of acute exercise on GLUT4 levels in peripheral blood mononuclear cells of sled dogs. Biochem. Biophys. Rep. 2, 45–49. http://dx.doi.org/10.1016/j.bbrep.2015.05.002.

Sharma, D., Verma, S., Vaidya, S., Kalia, K., Tiwari, V., 2018. Recent updates on GLP-1 agonists: Current advancements & challenges. Biomed. Pharmacother. 108, 952–962. http://dx.doi.org/10.1016/j.biopha.2018.08.088.

Siewe, N., Friedman, A., 2020. Increase hemoglobin level in severe malarial anemia while controlling parasitemia: A mathematical model. Math. Biosci. 326 (108374), http://dx.doi.org/10.1016/j.mbs.2020.108374.

Simo, R., Barbosa-Desongles, A., Lecube, A., Hernandez, C., Selva, D.M., 2012. Potential role of tumor necrosis factor-α in downregulating sex hormone–binding globulin. Diabetes 61, 372–382.

Stanley, T.L., Zanni, M.V., Johnsen, S., Rasheed, S., Makimura, H., Lee, H., et al., 2011. TNF-alpha antagonism with etanercept decreases glucose and increases the proportion of high molecular weight adiponectin in obese subjects with features of the metabolic syndrome. J. Clin. Endocrinol. Metab. 96 (1), E146–50. http://dx.doi.org/10.1210/jc.2010-1170.

Vieira, G., 2022. What are normal blood sugar levels? DiabetesStrong. https://diabetesstrong.com/what--are--normal--blood--sugar--levels/.

Villanueva-Peñacarrillo, M.L., Puente, J., Redondo, A., Clemente, F., Valverde, I., 2001. Effect of GLP-1 treatment on GLUT2 and GLUT4 expression in type 1 and type 2 rat diabetic models. Endocrine 15 (2), 241–248. http://dx.doi.org/10.1385/ENDO:15:2:241.

Virtamen, K.A., 2019. Activation of human brown adipose tissue (BAT): Focus on nutrition and eating. Handb. Exp. Pharmacol. 251, 349–357. http://dx.doi.org/10.1007/164_2018_136.

Wolfsdorf, J.I., Weinstein, D.A., 2012. Glycogen storage diseases. Goldman's Cecil Med. (Twenty-Fourth Ed.) 2 (214), 1354–1357. http://dx.doi.org/10.1016/B978-1-4377-1604-7.00214-1.

Zaki, M., Hussein, J., Ibrahim, A.M.M., Youness, E.R., 2020. Circulating plasma free fatty acids, insulin resistance and metabolic markers in obese women. Biomed. Pharmacol. J. 13 (4), http://dx.doi.org/10.13005/bpj/2034.

Zhang, Y., Parajuli, K.R., Fava, G.E., Gupta, R., Xu, W., Nguyen, L.U., et al., 2019. GLP-1 receptor in pancreatic α-cells regulates glucagon secretion in a glucose-dependent bidirectional manner. Diabetes 68 (1), 34–44. http://dx.doi.org/10.2337/db18-0317.

Zhou, H., Urso, C.J., Jadeja, V., 2020. Saturated fatty acids in obesity-associated inflammation. J. Inflamm. Res. 13, 1–14. http://dx.doi.org/10.2147/JIR.S229691.